The FEBS Journal

FEBS PRESS science publishing by scientists

Alternative [2Fe-2S] donor assemblies in the cytosol: GLRX3 and GLRX3-BOLA2 converge on NUBP1 maturation

Martina Masini[1,2], Rosanna Cuccaro[1,2] and Lucia Banci[1,2,3]

1 Department of Chemistry, University of Florence, Florence, Italy
2 Magnetic Resonance Center CERM, University of Florence, Florence, Italy
3 Consorzio Interuniversitario Risonanze Magnetiche di Metalloproteine (CIRMMP), Florence, Italy

Keywords
anamorsin; BOLA2; GLRX3; iron–sulfur cluster; NUBP1

Correspondence
M. Masini and L. Banci, Department of Chemistry, University of Florence, Via della Lastruccia 3, 50019 Sesto Fiorentino, Florence, Italy
Tel: +39 0554574196 and +39 0554574273
E-mail: martina.masini1@unifi.it and banci@cerm.unifi.it

(Received 13 April 2026, revised 3 July 2026, accepted 24 July 2026)

doi:10.1111/febs.70674

Iron–sulfur (Fe-S) cluster assembly in the cytosol relies on coordinated transfer of [2Fe-2S] precursors to scaffold proteins of the cytosolic iron–sulfur assembly (CIA) machinery. Human glutaredoxin 3 (GLRX3) functions as a central [2Fe-2S] cluster donor and can form a heterotrimeric complex with the BolA-like protein BOLA2, whose functional role in cluster trafficking remains unclear. Here, we directly compare the cluster donor properties of the GLRX3 homodimer with those of the GLRX3-BOLA2 heterotrimer in the maturation of the CIA scaffold nucleotide-binding protein 1 (NUBP1). Using a combination of UV–Vis spectroscopy, acid-labile iron and sulfide quantification, circular dichroism kinetics, and paramagnetic NMR, we show that both complexes support assembly of a canonical [4Fe-4S] cluster on the N-terminal site of NUBP1. The structural and spectroscopic features of the assembled cluster are indistinguishable between the two donor systems, and comparable levels of cluster incorporation are observed. Kinetic analysis reveals that cluster transfer proceeds with similar apparent rate constants for GLRX3 and GLRX3-BOLA2 under glutathione-supported conditions. The presence of the physiological electron donor anamorsin accelerates the GLRX3-mediated transfer but does not significantly affect the kinetics of the GLRX3-BOLA2 system, suggesting a shift in the rate-limiting step upon BOLA2 association. Together, these results show that GLRX3-BOLA2 is fully competent for [2Fe-2S] cluster delivery to NUBP1 and supports the formation of the same final [4Fe-4S] cluster observed upon GLRX3-mediated transfer. Rather than enhancing transfer efficiency, BOLA2 association appears to play a nonkinetic role, potentially related to cluster stabilization by modulating the electron transfer process under specific cellular conditions.

Introduction

Iron–sulfur (Fe-S) clusters are ancient and versatile cofactors that support essential cellular processes, including enzymatic catalysis, electron transfer, DNA replication and repair, and the regulation of gene expression and iron homeostasis [1–6]. Because of their chemical reactivity, the assembly and delivery of Fe-S clusters require dedicated and tightly regulated biosynthetic pathways. In eukaryotic cells, *de novo* Fe-S

Abbreviations
BOLA2, BolA-like protein 2; CD, circular dichroism; CIA, cytosolic iron–sulfur assembly; DTT, dithiothreitol; Fe-S, iron–sulfur; FPLC, fast protein liquid chromatography; GLRX3, glutaredoxin 3; GSH, glutathione; IPTG, isopropyl β-D-1-thiogalactopyranoside; ISC, iron–sulfur cluster (mitochondrial) assembly machinery; LB, Luria–Bertani; NMR, nuclear magnetic resonance; NUBP1, nucleotide-binding protein 1; TEV, tobacco etch virus; UV-Vis, ultraviolet–visible spectroscopy.

cluster synthesis is initiated by the mitochondrial ISC machinery, whose activity is required for the maturation of cytosolic and nuclear Fe-S proteins by the CIA machinery [7–10]. This mitochondrial contribution requires a mitochondrial export step involving the ABC transporter Atm1/ABCB7; however, the chemical nature of the exported sulfur-containing species remains debated [11–14]. Different models have been proposed, including the export of glutathione-associated sulfur species or glutathione-coordinated Fe-S-related intermediates, but whether any of these species represents the physiological substrate *in vivo* remains unresolved [11–14]. Once this mitochondrial-dependent input reaches the cytosolic compartment, Fe-S precursors must be safely handled, protected from degradation, and directed toward the appropriate CIA components for subsequent assembly and transfer to cytosolic and nuclear target proteins. Although the core components of the CIA pathway have been identified, several aspects of how Fe-S clusters are dynamically trafficked, remodeled, and protected in the cytosolic environment remain incompletely understood.

Within this cytosolic network, monothiol glutaredoxins and BolA-like proteins have emerged as key players in iron and Fe-S cluster metabolism [15]. Monothiol CGFS glutaredoxins, including human glutaredoxin 3 (GLRX3), bind [2Fe-2S] clusters in a glutathione (GSH)-dependent manner and function as mobile cluster carriers [2,15–19]. BolA-like proteins, characterized by a conserved BolA domain, frequently associate with monothiol glutaredoxins to form heterocomplexes capable of coordinating bridged [2Fe-2S] clusters [20–22]. This interaction represents a conserved strategy for integrating redox chemistry, iron sensing, and Fe-S cluster trafficking.

In human cells, GLRX3 exists in two distinct cluster-bound assemblies: a canonical GLRX3 homodimer and a heterotrimeric complex formed with BOLA2, in which two BOLA2 molecules associate with the two Grx domains of GLRX3 [16]. Structural and spectroscopic studies have shown that the GLRX3-BOLA2 complex represents an alternative cluster-binding architecture relative to the GLRX3 homodimeric form [16,20,23]. Importantly, interactions between glutaredoxin-like and BolA-like proteins have been proposed to stabilize bound [2Fe-2S] clusters and modulate their reactivity, potentially linking Fe-S cluster availability to cellular redox and iron status [24–26]. Despite these insights, the functional implications of this alternative assembly mode within the CIA pathway remain incompletely understood.

A central step in cytosolic Fe-S protein maturation is the assembly of [4Fe-4S] clusters on the essential CIA scaffold protein NUBP1 (Nbp35 in yeast) [27–30]. NUBP1 receives [2Fe-2S] clusters that are reductively coupled to generate a [4Fe-4S] cluster, a process that requires both a suitable cluster donor and an electron source. GLRX3 has been firmly established as a direct [2Fe-2S] cluster donor to NUBP1, acting in cooperation with the electron transfer protein anamorsin [23,28]. In this context, the formation of alternative GLRX3-containing assemblies raises the possibility that distinct donor complexes may contribute differently to NUBP1 maturation.

Consistent with this view, several models have been proposed to explain the physiological function of BOLA2 in cytosolic Fe-S cluster trafficking. One model suggests that association with BOLA2 stabilizes GLRX3-bound clusters and protects them from oxidative degradation, thereby preserving a transferable pool of Fe-S cofactors under fluctuating cellular conditions [15]. Other genetic and biochemical evidence suggests that Fe-S cluster trafficking is supported by partially redundant protein systems, in which multiple cluster carriers coexist and can contribute to cluster delivery under different physiological conditions [31]. This functional diversity is further modulated by glutathione, which plays a multifaceted role as a cluster ligand, redox buffer, and potential electron donor, influencing both cluster chirality and transfer chemistry [32–34]. Collectively, these observations highlight the need to directly assess how different GLRX3-based assemblies contribute to cluster delivery within the CIA pathway.

In this study, we directly compare the cluster donor properties of the GLRX3 homodimer and the GLRX3-BOLA2 heterotrimer in the context of NUBP1 maturation. Using complementary biochemical and spectroscopic approaches, we evaluate their ability to support [4Fe-4S] cluster assembly and their dependence on electron donation by anamorsin. By defining the functional overlap and distinctions between these two donor systems, our work contributes to better defining the mechanistic framework of cytosolic Fe-S cluster biogenesis and provides insight into how robustness and regulation are integrated within the CIA machinery. Given the central importance of Fe-S cluster metabolism in human physiology and their involvement in pathological conditions [3,4,35,36], these findings advance our understanding of the molecular principles governing cellular iron–sulfur homeostasis.

Results

GLRX3-BOLA2$_2$ heterotrimer and GLRX3$_2$ homodimer support comparable endpoint [4Fe-4S] cluster assembly on NUBP1

We evaluated the ability of the GLRX3-BOLA2$_2$ complex to donate [2Fe-2S] clusters to the scaffold protein NUBP1, where $[4Fe\text{-}4S]^{2+}$ clusters are assembled via reductive coupling of two $[2Fe\text{-}2S]^{2+}$ units. To restrict cluster coordination to a single, defined site, we employed a mutated form of NUBP1, hereafter referred to as NUBP1-NT, in which the C-terminal CPXC cluster-binding motif is inactivated by substitution of Cys235 and Cys238 with alanine residues. This construct retains the N-terminal $CX_{13}CX2CX_5C$ cluster-binding motif and allows selective monitoring of $[4Fe\text{-}4S]^{2+}$ cluster formation at the N-terminal site [27]. The NUBP1-C235A/C238A construct was previously characterized and shown to preserve protein folding, as assessed by CD and NMR spectroscopy, while retaining the spectroscopic features associated with N-terminal [4Fe-4S] cluster coordination [27]. The absence of the C-terminal site prevents formation of the bridging cluster-associated dimeric architecture and therefore allows the N-terminal cluster assembly event to be monitored without contributions from the C-terminal cluster-binding site.

Cluster transfer reactions were performed under anaerobic conditions by incubating apo NUBP1-NT with chemically reconstituted $[2Fe\text{-}2S]_2$-GLRX3$_2$ or $[2Fe\text{-}2S]_2$-(GLRX3-BOLA2$_2$) complexes in a 1:2 acceptor-to-donor molar ratio. Incubations were carried out for 1 h at room temperature in the presence of 15 mM reduced glutathione (GSH), which acts as both the coordinating and reducing cluster moiety and as electron donor in the [4Fe-4S] cluster coupling. Following incubation, NUBP1 was separated from the donor complexes by immobilized metal affinity chromatography using His GraviTrap columns, as described in the Materials and Methods section.

UV–Vis spectra of the eluted NUBP1 (Fig. 1A) revealed the appearance of a broad absorption band centered at 410 nm (Fig. 1A), consistent with $[4Fe\text{-}4S]^{2+}$ cluster coordination. Importantly, both the intensity and shape of the absorption band were nearly identical between the two donor systems, indicating comparable endpoint levels of [4Fe-4S] cluster assembly under the donor-normalized conditions used. Consistent with effective cluster transfer, comparison of the UV–Vis spectra of the donor complexes before and after the reaction showed a concomitant decrease in the characteristic $[2Fe\text{-}2S]^{2+}$ absorbance features. In the case of GLRX3-BOLA2$_2$, this reduction was clearly observed at ~ 410 nm following incubation with NUBP1 (Fig. 1B), while an analogous decrease was detected for the GLRX3$_2$ homodimer at ~ 410 nm (Fig. 1C), confirming partial consumption of the donor-bound [2Fe-2S] clusters during the transfer process.

To quantify the extent of cluster incorporation, acid-labile iron and sulfide contents were determined for both sets of samples (Table 1). NUBP1 samples that received clusters from GLRX3-BOLA2$_2$ contained 2.5 ± 0.2 mol of Fe and 2.7 ± 0.3 mol of S per mol of protein, and comparable values were obtained for samples loaded via the GLRX3$_2$ homodimer (2.5 ± 0.1 mol Fe and 2.5 ± 0.3 mol S). These values correspond to approximately 0.6 equivalents of [4Fe-4S] cluster per protein, indicating partial but significant cluster incorporation under the *in vitro* conditions used. The close agreement between the two donor systems further supports comparable endpoint [4Fe-4S] cluster incorporation under the donor-normalized conditions used.

To further characterize the kinetics of cluster transfer, time-resolved circular dichroism (CD) spectra were acquired during the incubation of donor and acceptor proteins. The time-dependent variation of a characteristic CD signal of the donor complex was monitored to follow the progress of the cluster transfer reaction. For both the GLRX3-BOLA2$_2$ complex and the GLRX3$_2$ homodimer, the CD signals decreased progressively during the reaction and reached a plateau within approximately 40 min. The kinetic traces were fitted using a monoexponential decay model to obtain apparent rate constants for the transfer process. Under these conditions, the reaction performed by $[2Fe\text{-}2S]_2$-GLRX3$_2$ (Fig. 2B) displayed an apparent rate constant of $k = 1.24 \pm 0.31 \times 10^{-3}$ s^{-1}, whereas with the $[2Fe\text{-}2S]_2$-(GLRX3-BOLA2$_2$) system (Fig. 2A) it was $k = 1.47 \pm 0.15 \times 10^{-3}$ s^{-1}. The similar value of this kinetic constant indicates that the presence of BOLA2 does not significantly influence the overall rate of cluster transfer to NUBP1.

1D paramagnetic ^{1}H NMR spectra of NUBP1 samples after incubation with either holo GLRX3$_2$ or holo GLRX3-BOLA2$_2$ (Fig. 3) are very similar, featuring a set of hyperfine-shifted resonances in the 18–11 ppm region. These signals correspond to βCH$_2$ protons of the four cysteine residues that coordinate the [4Fe-4S] cluster at the N-terminal site of NUBP1. The similarity in chemical shift patterns and relative intensities confirmed that both donor systems result in equivalent cluster assembly and that the iron–sulfur cluster has the same coordination structure in the two samples.

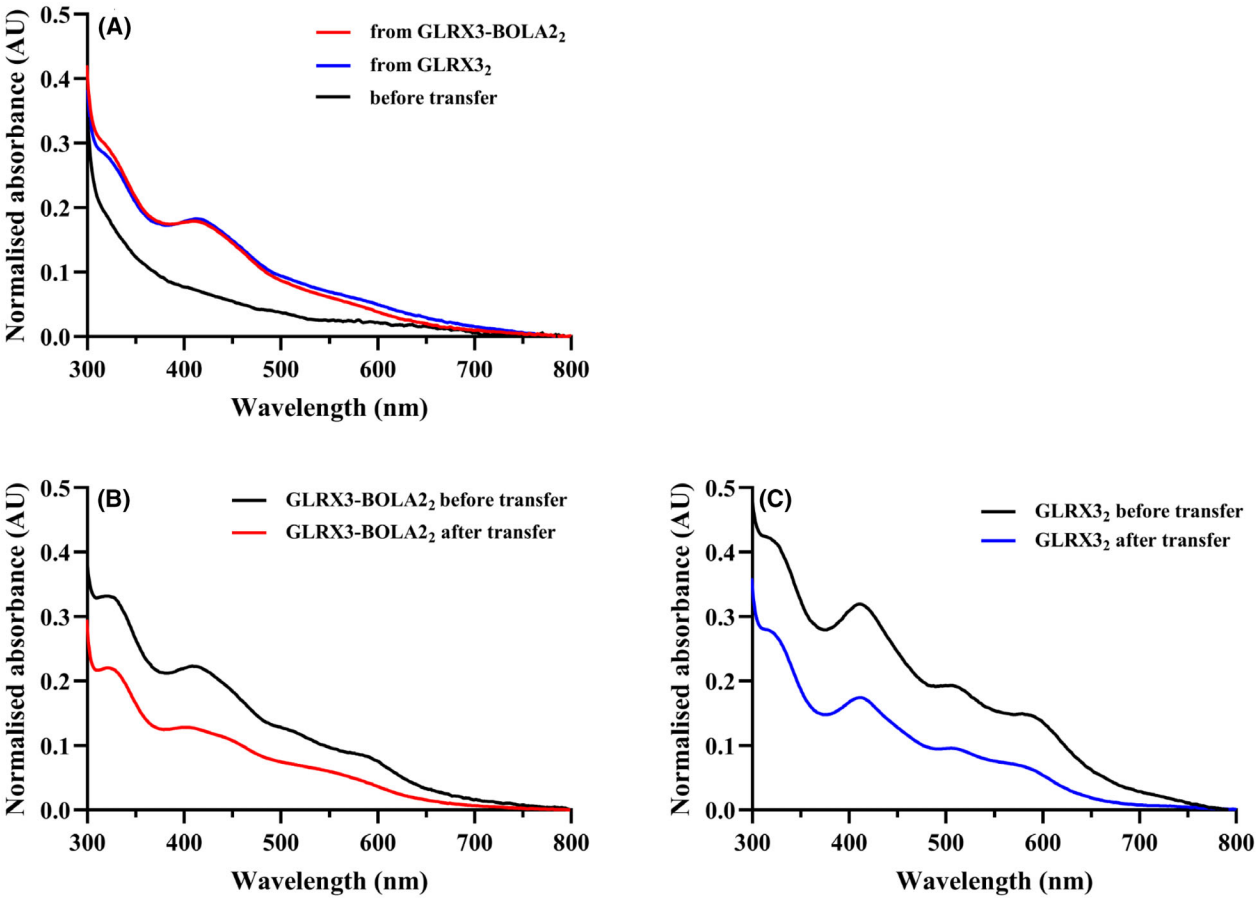

Fig. 1. GLRX3-BOLA2$_2$ and GLRX3$_2$ support comparable [4Fe-4S] cluster assembly on NUBP1. (A) UV–Vis spectra of NUBP1 after incubation with [2Fe-2S]$_2$-GLRX3$_2$ and [2Fe-2S]$_2$-(GLRX3-BOLA2$_2$); similar 410 nm absorbance intensity indicating [4Fe-4S] cluster formation. (B) UV–Vis spectra of [2Fe-2S]$_2$-(GLRX3-BOLA2$_2$) before (black) and after (red) reaction with NUBP1. (C) UV–Vis spectra of [2Fe-2S]$_2$-GLRX3$_2$ before (black) and after (blue) reaction with NUBP1. Representative UV–Vis spectra from one of $n = 3$ independent experiments are shown; all replicates gave comparable spectral features.

Table 1. Quantification of acid-labile Fe and S in NUBP1 after cluster transfer. Values are reported as mean ± SD from $n = 3$ independent experiments.

Donor complex	Fe (mol/mol NUBP1)	S (mol/mol NUBP1)	[4Fe–4S] equivalents
GLRX3$_2$	2.5 ± 0.1	2.5 ± 0.3	0.63 ± 0.04
GLRX3-BOLA2$_2$	2.5 ± 0.2	2.7 ± 0.3	0.65 ± 0.05

Together, these results demonstrate that the GLRX3-BOLA2$_2$ complex is fully competent for [2Fe-2S] cluster donation to NUBP1, and supports comparable endpoint [4Fe-4S] cluster assembly to the GLRX3$_2$ homodimer under the donor-normalized reducing conditions used.

Role of anamorsin in [4Fe-4S] cluster assembly

Previous studies [23,28] have established that anamorsin functions as the physiological electron donor required for reductive coupling in the [4Fe-4S] cluster assembly on NUBP1. Building on this framework, we sought to determine whether anamorsin similarly supports [4Fe-4S] cluster formation when the [2Fe-2S] clusters are delivered by the GLRX3-BOLA2 heterotrimer instead of by the GLRX3 homodimer. To address this question, we extended our *in vitro* reconstitution assays to include anamorsin in cluster transfer reactions between GLRX3-BOLA2 and NUBP1. By directly comparing outcomes in the presence and absence of anamorsin, we assessed whether electron donation by anamorsin affects the reductive coupling process when GLRX3-BOLA2 serves as the [2Fe-2S] cluster donor.

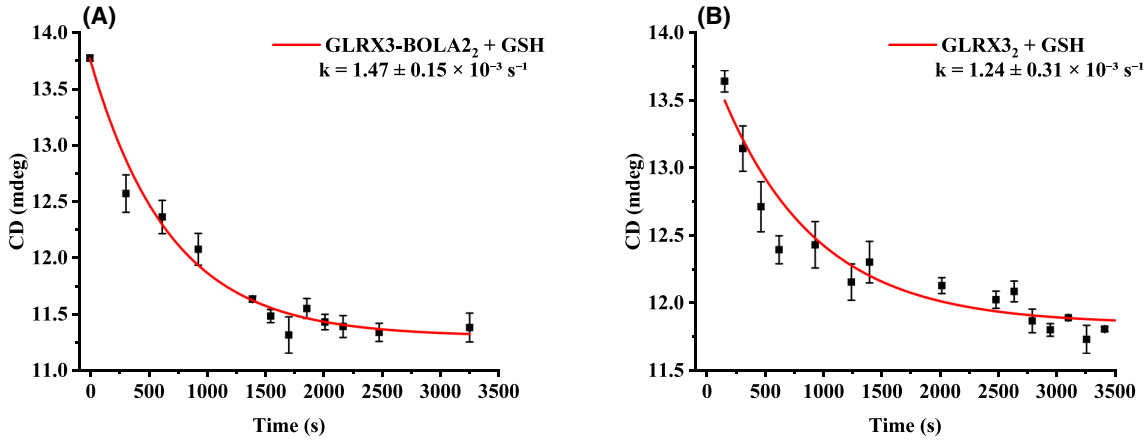

Fig. 2. GLRX3-BOLA2$_2$ and GLRX3$_2$ display comparable cluster transfer kinetics under glutathione-supported conditions. Kinetic analysis of [2Fe-2S] cluster transfer to NUBP1 was monitored by time-resolved circular dichroism (CD) spectroscopy. Time-resolved CD spectra were recorded during the anaerobic incubation of apo NUBP1-NT with either the GLRX3-BOLA2$_2$ complex (A) or the GLRX3 homodimer (B) in the presence of 15 mM GSH. The evolution of the CD signal at 560 nm was monitored over time to follow the transfer reaction and a monoexponential fit of the kinetic traces was used to determine the apparent rate constants (k_{tr}). Comparable values were obtained for the two donor complexes, with $k = 1.47 \times 10^{-3}$ s^{-1} for GLRX3-BOLA2$_2$ and $k = 10^{-3}$ s^{-1} for GLRX3$_2$, indicating similar transfer kinetics under glutathione-supported conditions. Data points represent the mean of $n = 2$ independent experiments; error bars indicate SD. Reported k values are mean ± SD from the same independent experiments.

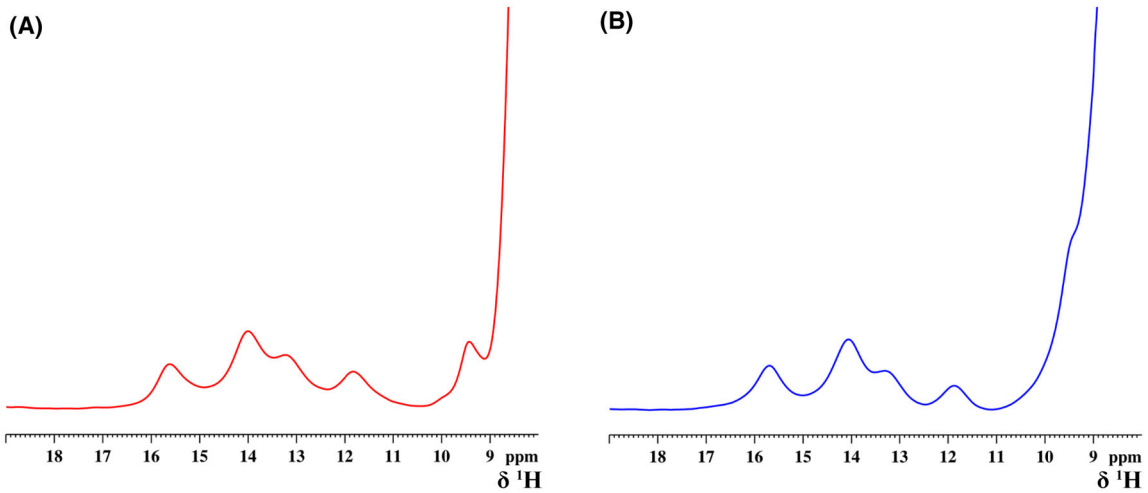

Fig. 3. Paramagnetic NMR confirms the same [4Fe-4S] cluster coordination on NUBP1. Paramagnetic NMR spectra of NUBP1 after incubation with GLRX3-BOLA2$_2$ (A) and GLRX3$_2$ (B); the four hyperfine shifted peaks in the region of 10 to 20 ppm indicate [4Fe-4S]-bound cysteinyl protons. Representative 1D paramagnetic ^{1}H NMR spectra from one of $n = 3$ independent experiments are shown; all replicates gave comparable hyperfine-shifted resonance patterns.

UV–Vis spectra of NUBP1 obtained after incubation with holo GLRX3-BOLA2$_2$ in the presence of anamorsin displayed a well-defined absorption band centered at ~ 410 nm (Fig. 4A, purple trace), consistent with the formation of a [4Fe-4S]$^{2+}$ cluster. Notably, the spectral features closely match those observed under glutathione-supported conditions and with the GLRX3$_2$ homodimer, indicating that neither the nature of the electron donor nor the presence of BOLA2 affects the structural properties of the assembled cluster. These results indicate that reductive coupling of the two [2Fe-2S] precursors can occur under both conditions, yielding comparable endpoint levels of NUBP1 cluster incorporation under the tested *in vitro* conditions. Paramagnetic ^{1}H NMR spectra of NUBP1 isolated after the two modes of reactions

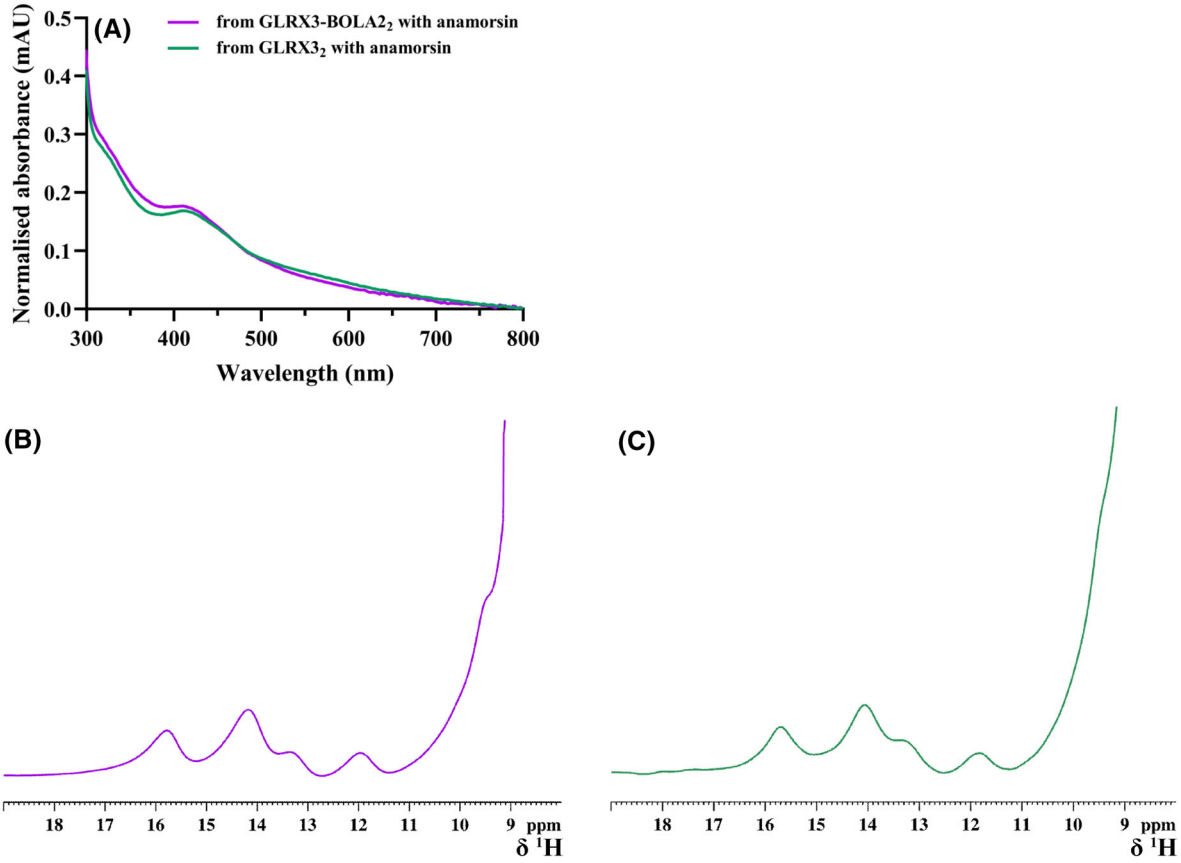

Fig. 4. Anamorsin supports [4Fe-4S] cluster assembly without significantly altering the spectroscopic features of the assembled cluster. (A) UV–Vis spectra of NUBP1 after incubation with GLRX3-BOLA2 and anamorsin (purple) or GLRX3$_2$ and anamorsin (green). Comparison of 410 nm absorbance intensities. (B) Paramagnetic NMR spectra of NUBP1 after transfer from holo GLRX3-BOLA2$_2$ plus anamorsin (purple). (C) Paramagnetic NMR spectra of NUBP1 after transfer from holo GLRX3$_2$ plus anamorsin (green). Representative UV–Vis and 1D paramagnetic ^{1}H NMR spectra from one of $n = 3$ independent experiments are shown; all replicates gave comparable spectral features.

supported this interpretation (Fig. 4B and Fig. 4C). The spectra obtained after incubation with anamorsin showed the well-defined set of hyperfine-shifted resonances between 10 and 20 ppm, typical of [4Fe-4S]-bound cysteinyl protons, as observed for the reaction with GSH. Importantly, the chemical shift pattern was nearly identical between GLRX3$_2$- and GLRX3-BOLA2-derived samples, indicating that the coordination geometry of the final cluster is conserved.

To quantify the extent of cluster incorporation, acid-labile Fe and S were determined for NUBP1 samples obtained under each condition (Table 2). NUBP1 loaded in the presence of anamorsin contained approximately 2.5 ± 0.1 mol Fe and 2.6 ± 0.2 mol S per mol of protein for both donor systems. No significant differences were detected between the GLRX3-BOLA2$_2$ and GLRX3$_2$ donors in either condition.

The effect of the physiological electron donor anamorsin on the kinetics of cluster assembly was also investigated by performing analogous CD experiments in its presence. In reactions performed by GLRX3$_2$, the addition of anamorsin led to an increase in the apparent rate constant, yielding $k = 2.87 \pm 0.60 \times 10^{-3}$ s^{-1} (Fig. 5B), approximately twofold higher than that observed in the

Table 2. Quantification of acid-labile Fe and S in NUBP1 after cluster transfer in the presence of anamorsin. Values are reported as mean ± SD from $n = 3$ independent experiments.

Donor complex	Electron donor	Fe (mol/mol NUBP1)	S (mol/mol NUBP1)	[4Fe–4S] equivalents
GLRX3$_2$	anamorsin	2.5 ± 0.1	2.5 ± 0.2	0.63 ± 0.03
GLRX3$_2$	GSH	2.5 ± 0.1	2.5 ± 0.3	0.63 ± 0.04
GLRX3-BOLA2$_2$	anamorsin	2.6 ± 0.1	2.6 ± 0.2	0.65 ± 0.03
GLRX3-BOLA2$_2$	GSH	2.5 ± 0.2	2.7 ± 0.3	0.65 ± 0.05

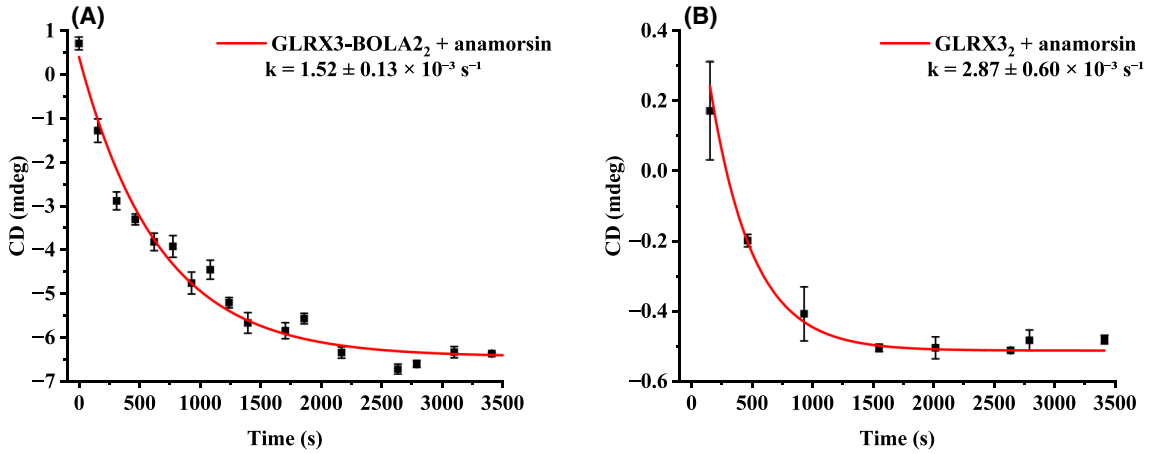

Fig. 5. Distinct kinetic effects of anamorsin on GLRX3- and GLRX3-BOLA2-mediated cluster transfer to NUBP1. Time-resolved CD measurements monitoring the transfer of [2Fe-2S] clusters from GLRX3-BOLA2$_2$ (A) or GLRX3$_2$ (B) to apo NUBP1-NT in the presence of the physiological electron donor anamorsin. Monoexponential fits of the kinetic data were used to determine the apparent rate constants. The GLRX3-mediated reaction exhibits $k = 2.87 \times 10^{-3}$ s^{-1}, approximately twofold higher than in the absence of anamorsin, consistent with its role as a physiological electron donor. In contrast, the GLRX3-BOLA2$_2$ system shows a similar rate constant ($k = 1.52 \times 10^{-3}$ s^{-1}), indicating that the GLRX3-BOLA2$_2$ system does not display anamorsin-dependent acceleration. Data points represent the mean of $n = 2$ independent experiments; error bars indicate SD. Reported k values are mean ± SD from the same independent experiments.

glutathione-containing system. This result is consistent with the established role of anamorsin as the physiological electron donor involved in the reductive coupling step during [4Fe-4S] cluster formation on NUBP1. In contrast, when the GLRX3-BOLA2$_2$ complex was used as cluster donor (Fig. 5A), the apparent rate constant obtained in the presence of anamorsin ($k = 1.52 \pm 0.13 \times 10^{-3}$ s^{-1}) was similar to that measured in the absence of the protein electron donor. This observation indicates that the association of BOLA2 with GLRX3 in the presence of anamorsin does not lead to a significant acceleration of the overall transfer reaction.

Taken together, these kinetic measurements show that, although anamorsin enhances the rate of GLRX3-mediated cluster transfer, the GLRX3-BOLA2$_2$ complex displays similar apparent rate constants in the presence of either anamorsin or glutathione. This suggests that electron transfer is not the rate-limiting step when GLRX3-BOLA2$_2$ acts as the [2Fe-2S] cluster donor.

Overall, these data show that the GLRX3-BOLA2$_2$ complex provides the cluster precursors required for NUBP1 maturation and supports formation of the same final [4Fe-4S] cluster observed with GLRX3-mediated transfer. However, unlike the GLRX3 homodimer, the GLRX3-BOLA2$_2$ complex does not display anamorsin-dependent acceleration, indicating a distinct kinetic dependence on the electron donor.

Discussion

Iron–sulfur cluster trafficking in the cytosol relies on a coordinated network of carrier proteins that ensure the safe delivery of highly reactive cofactors to their target proteins. Within this network, the monothiol glutaredoxin GLRX3 has been established as a central [2Fe-2S] cluster donor for components of the cytosolic iron–sulfur assembly (CIA) machinery [3,27]. The ability of GLRX3 to form a stable heterotrimeric complex with BOLA2 raises the question of whether this alternative assembly simply preserves the canonical GLRX3 donor function or instead modulates specific steps of cluster trafficking, such as cluster stabilization, electron dependence, or productive interaction with downstream CIA components [20,23].

In this work, we directly compared the cluster donor properties of the GLRX3 homodimer and the GLRX3-BOLA2 heterotrimer in the context of NUBP1 maturation. Multiple spectroscopic approaches consistently show that both complexes support the formation of a canonical [4Fe-4S] cluster on the N-terminal binding site of NUBP1. UV–Vis spectra display the characteristic absorption feature at ~ 410 nm associated with [4Fe-4S]$^{2+}$ cluster coordination, while paramagnetic NMR spectra show the expected set of hyperfine-shifted resonances arising from cysteinyl ligands of the cluster. The close similarity between spectra obtained using GLRX3$_2$ and GLRX3-BOLA2$_2$ indicates that the structural nature

of the cluster assembled on NUBP1 is conserved regardless of the donor system. This conclusion is further supported by iron and sulfide quantification, which shows comparable incorporation of a [4Fe-4S] cluster on NUBP1 under all tested conditions. Together, these data establish that GLRX3-BOLA2 is competent to supply the [2Fe-2S] precursors required for reductive coupling on NUBP1.

The interpretation of this result is facilitated by the use of the NUBP1-NT construct, which allows selective monitoring of [4Fe-4S] cluster assembly at the N-terminal site. This construct lacks the functional C-terminal CPXC cluster-binding motif but has been previously shown to preserve the overall folding of NUBP1 and the spectroscopic features of the N-terminal [4Fe-4S]-bound form [27]. It therefore provides a suitable model to isolate the cluster assembly event addressed in this study. At the same time, this simplified system does not reproduce the full architecture of native NUBP1. In the full-length protein, the C-terminal motif contributes to the formation of a dimeric scaffold through coordination of a bridging cluster and may influence site occupancy, donor recognition, or communication between cluster-binding regions [27]. Thus, while our data demonstrate that both GLRX3 and GLRX3-BOLA2 promote [4Fe-4S] cluster formation at the N-terminal site, additional effects involving the C-terminal cluster and the complete NUBP1/NUBP2 scaffold may occur in the native system.

The extent of cluster incorporation observed in our endpoint assays should also be considered within this mechanistic framework. Under all tested conditions, NUBP1 reaches partial but reproducible [4Fe-4S] cluster loading. Substoichiometric Fe-S cluster incorporation is commonly observed in *in vitro* reconstitution and transfer experiments, even under optimized anaerobic conditions. Studies of the yeast Cfd1-Nbp35 scaffold further indicate that Fe-S cluster loading and kinetic lability are strongly influenced by scaffold architecture, nucleotide binding, and protein–protein interactions [37,38]. Partial cluster incorporation has also been reported for NUBP1, where the final cluster occupancy depends on the cluster-binding site and on the reducing conditions used [27,28]. More generally, studies on cytosolic Fe-S cluster trafficking and CIA scaffold proteins indicate that cluster transfer reactions are governed by both kinetic and thermodynamic factors and may not proceed quantitatively in simplified systems lacking the full set of physiological partners [39–41].

In the case of NUBP1-NT, formation of a [4Fe-4S] cluster requires two sequential [2Fe-2S] delivery events followed by reductive coupling. Under the transfer conditions used here, the isolated NUBP1 product displays spectroscopic signatures consistent with [4Fe-4S] cluster formation, whereas no stable [2Fe-2S]-bound NUBP1 intermediate is detected at the endpoint. The partial occupancy therefore does not appear to reflect accumulation of a half-converted NUBP1 intermediate, but rather the fraction of NUBP1 molecules in which both [2Fe-2S] delivery events and reductive coupling have proceeded to completion. In the isolated *in vitro* system used here, this endpoint may reflect an apparent equilibrium between donor-bound [2Fe-2S] clusters and acceptor-bound [4Fe-4S] clusters. *In vivo*, subsequent transfer of the newly assembled [4Fe-4S] cluster to downstream CIA components or client proteins could provide an additional thermodynamic and kinetic drive for further cluster assembly.

The kinetic data further refine this picture by revealing a difference between the two donor systems in their dependence on electron transfer. When GLRX3 serves as the donor, the presence of the physiological electron donor anamorsin accelerates cluster transfer relative to glutathione-supported conditions, in agreement with the role of anamorsin in the CIA electron transfer chain [23,28]. In contrast, GLRX3-BOLA2-mediated transfer proceeds with similar apparent rate constants in the presence of either anamorsin or glutathione. Thus, BOLA2 association does not enhance the overall rate of cluster transfer to NUBP1 under the conditions tested. Rather, the lack of anamorsin-dependent acceleration suggests that, in the GLRX3-BOLA2 system, electron delivery is no longer the dominant rate-limiting step, and that other processes, such as cluster release or productive donor-acceptor recognition, may become more relevant for the overall reaction rate.

This interpretation is consistent with the known stabilizing effect of BOLA2 on GLRX3-bound [2Fe-2S] clusters [16,20]. Stabilization of the donor-bound cluster may preserve a transferable cluster pool, but it may also modify the energetic balance of the transfer reaction and the extent to which electron delivery accelerates the process. Cluster transfer itself is expected to involve ligand exchange, as cysteine residues from NUBP1 must replace donor ligands in the [2Fe-2S] coordination sphere. Therefore, some reorganization of the donor coordination environment is an intrinsic part of the transfer mechanism. The present data show that GLRX3-BOLA2 preparations are competent donors for NUBP1 maturation, but they do not define whether BOLA2 remains associated with GLRX3 throughout the entire transfer event or whether transient dissociation or rearrangement occurs during cluster delivery.

Taken together, these findings indicate that GLRX3-BOLA2 functions as an alternative GLRX3-containing [2Fe-2S] donor complex that converges on the same NUBP1 maturation outcome as GLRX3 alone, while displaying a distinct kinetic dependence on the electron donor. Rather than acting primarily by increasing transfer efficiency, BOLA2 appears to modulate the properties of the GLRX3-bound cluster, potentially balancing cluster stabilization with transfer competence. This behavior may provide a functional advantage in the cytosolic Fe-S trafficking network, where cluster donors must both protect labile cofactors and release them efficiently to appropriate acceptors.

In the cellular context, NUBP1 is not an endpoint for Fe-S cluster trafficking, but part of a broader CIA network in which newly assembled [4Fe-4S] clusters are transferred to downstream maturation factors and ultimately to client proteins. Therefore, NUBP1 cluster occupancy is expected to reflect a dynamic steady state determined by upstream cluster supply, donor-to-acceptor transfer equilibria, electron availability, and downstream cluster consumption. This view is consistent with studies in yeast and mammalian systems showing that cytosolic Fe-S cluster trafficking depends on coordinated interactions between Grx/BolA-type carriers, the Nbp35/Cfd1 or NUBP1/NUBP2 scaffold, and downstream CIA targeting factors [39,40,42–44].

Accordingly, when downstream demand is low, NUBP1 occupancy may be governed mainly by donor-to-acceptor equilibria. Conversely, when cellular demand for Fe-S clusters increases, continuous removal of NUBP1-bound [4Fe-4S] clusters by downstream acceptors could shift the apparent equilibrium and promote further cluster delivery from upstream donor systems. In this framework, the coexistence of GLRX3 homodimers and GLRX3-BOLA2 heterotrimers may contribute to the robustness of cytosolic Fe-S trafficking by providing alternative donor assemblies whose relative contribution depends on cluster availability, electron-transfer conditions, and downstream demand.

While these findings provide a consistent *in vitro* framework, further studies will be required to establish how GLRX3 and GLRX3-BOLA2 contribute to Fe-S cluster trafficking in the cellular context and how the balance between these donor assemblies is regulated in response to changing cellular conditions.

Materials and methods

Protein expression and purification

The proteins used in this study were obtained through heterologous expression in *E. coli*, using different cell lines and vectors. GLRX3 and BOLA2 were produced according to previously published procedures [20,27,28]. To selectively probe [4Fe-4S] cluster assembly at the N-terminal site of NUBP1, we employed the NUBP1-C235A/C238A variant, hereafter referred to as NUBP1-NT, in which the C-terminal CPXC cluster-binding motif was inactivated. Based on our previous finding that GLRX3 donates [2Fe-2S] clusters exclusively to the N-terminal domain of NUBP1, cysteine residues Cys235 and Cys238 were substituted with alanine, thereby abolishing coordination of the C-terminal [4Fe-4S] cluster that normally bridges two NUBP1 subunits. This modification results in a monomeric form of NUBP1 retaining only the N-terminal [4Fe-4S] cluster-binding site. The mutant protein was expressed and purified following established protocols described previously [27]. BL21(DE3)-RIPL CodonPlus competent cells (Agilent Technologies, Santa Clara, CA, USA) were transformed with pETG20A (Novagen, Madison, WI, USA) plasmid containing N-terminal His_6-TRX-tagged GLRX3 gene. Native BOLA2 was expressed in BL21(DE3)-Gold (Agilent Technologies, USA) competent cells, which were transformed with pET21A plasmid (Novagen), while His_6-tagged NUBP1_NT was obtained by transforming BL21 (DE3) competent cells (Agilent Technologies, USA) with a pDUET plasmid (Novagen).

All cells were cultivated at 37 °C in Luria–Bertani (LB) medium supplemented with the appropriate antibiotics, shaking at 180 rpm. Protein expression was induced at OD_{600} = 0.6–0.8, by adding isopropyl β-D-1-thiogalactopyranoside (IPTG, Sigma-Aldrich, St. Louis, MO, USA) and $FeCl_3$ when needed and then shaking at 120 rpm for different durations and at different temperatures (Table 3).

The cell pellets were resuspended in the respective binding buffers and cell lysis was performed by sonication. All the proteins were purified by fast protein liquid chromatography (FPLC), using a HisTrap FF column (Cytiva, Marlborough, MA, USA) or HiTrap cation exchange resin column (Cytiva, USA) for BOLA2, following previously reported protocols [20,27,28]. The cleavage of the tags was performed by adding tobacco etch virus protease (TEV), produced in-house, overnight at room temperature, and then the tag was separated from the cleaved protein using a HisTrap FF column (Cytiva, USA).

Table 3. Conditions for protein expression induction.

Protein	Expression induction	Temperature	Time
GLRX3	0.5 mM IPTG; 0.25 mM $FeCl_3$	17 °C	overnight
BOLA2	0.5 mM IPTG	25 °C	5 h
His_6-tagged NUBP1_NT	0.5 mM IPTG; 0.25 mM $FeCl_3$	21 °C	overnight
Anamorsin	0.2 mM IPTG; 0.25 mM $FeCl_3$	25 °C	4 h

Chemical reconstitution

Holo protein complexes were chemically reconstituted overnight at room temperature under strictly anaerobic conditions in a glovebox (O_2 < 1 ppm), using thoroughly deoxygenated buffers and reagents. Reconstitution was carried out at a protein concentration of ~ 50 μM in 50 mM Tris–HCl buffer (pH 8.0), 150 mM NaCl, supplemented with 5 mM glutathione (GSH), and 5 mM dithiothreitol (DTT), by stepwise addition of $FeCl_3$ and Na_2S. Excess reagents were removed anaerobically using PD-10 desalting columns (Cytiva, USA). Unless otherwise stated, all subsequent experiments were performed in degassed 50 mM Tris–HCl (pH 8.0), 150 mM NaCl.

Cluster transfer reactions from $GLRX3_2$ and $GLRX3\text{-}BOLA2_2$ complex to apo NUBP1

Cluster transfer reactions were carried out under strictly anaerobic conditions inside a glovebox (O_2 < 1 ppm), using deoxygenated buffers. Apo NUBP1-NT was incubated with chemically reconstituted holo donor complexes in phosphate buffer (50 mM sodium phosphate, pH 8.0, 300 mM NaCl) for 1 h at room temperature, in a 1 : 2 acceptor-to-donor molar ratio. Prior to transfer assays, holo GLRX3 and GLRX3-BOLA2 donor preparations were normalized according to their cluster content, estimated from the intensity of the characteristic [2Fe-2S] absorption band at 410 nm. This ensured that comparable amounts of spectroscopically detectable donor-bound [2Fe-2S] cluster were added to the reactions performed with the two donor systems. Typical protein concentrations ranged from 80 to 100 μM for NUBP1-NT. Reactions were performed in the presence of 15 mM reduced glutathione (GSH) or, when indicated, with anamorsin added in equimolar ratio relative to the donor complex. Following incubation, NUBP1-NT was separated from donor proteins by immobilized metal affinity chromatography using a HisTrap column (Cytiva, USA) and eluted with phosphate buffer containing a high concentration of imidazole. The eluted protein was subsequently subjected to buffer exchange into 50 mM Tris–HCl (pH 8.0), 150 mM NaCl using a PD-10 desalting column to remove imidazole and restore conditions suitable for spectroscopic analyses.

Biochemical and spectroscopic studies

UV–Vis spectroscopy and 1H 1D paramagnetic NMR experiments were performed to assess [4Fe-4S] cluster assembly on NUBP1. UV–Vis spectra were recorded at room temperature using a Cary 50 spectrophotometer (Agilent Technologies, USA) in quartz cuvettes with 1-cm path length.

Time-resolved circular dichroism (CD) spectroscopy was performed on a JASCO J-810 spectropolarimeter (JASCO Inc., Tokyo, Japan) to monitor cluster transfer kinetics. Measurements were carried out under the same buffer conditions used for the cluster transfer reactions (50 mM sodium phosphate buffer, pH 8.0, 300 mM NaCl), supplemented with either 15 mM GSH or anamorsin. The CD signal at 560 nm, characteristic of the $[2Fe\text{-}2S]^{2+}$ cluster environment, was monitored over time. Kinetic traces were fitted to a monoexponential decay model using OriginPro software to obtain apparent rate constants (k). Reported values represent the mean ± standard deviation of at least two independent experiments.

1H 1D paramagnetic NMR spectra were acquired on a Bruker Avance spectrometer (Bruker BioSpin, Billerica, MA, USA) operating at 400 MHz 1H Larmor frequency, at 298 K. Samples were prepared in 50 mM Tris–HCl buffer (pH 8.0), 150 mM NaCl, supplemented with 10% (v/v) D_2O, 5 mM GSH, and 5 mM DTT. Water suppression was achieved using fast repetition experiments with selective irradiation. Spectra were processed using standard procedures. Acid-labile iron and sulfide contents were quantified using standard colorimetric assays based on ferrozine and methylene blue methods, respectively, as previously described [27]. All measurements were performed on at least two independent samples and showed consistent results.

Acknowledgements

The authors acknowledge the support by the Italian Ministry for University and Research (MUR, Rome, Italy; FOE funding) to the CERM/CIRMMP Italian Centre of Instruct-ERIC, an ESFRI Landmark. Support is also acknowledged from the project 'Potentiating the Italian Capacity for Structural Biology Services in Instruct Eric (ITACA.SB)' (Project n° IR0000009) within the call MUR 3264/2021 PNRR M4/C2/L3.1.1, funded by the European Union NextGenerationEU. The authors also acknowledge Dr. Francesca Camponeschi for her supervision and contributions during the early stages of the project.

Conflicts of interest

The authors declare no conflicts of interest.

Author contributions

MM performed experiments, analyzed data, and wrote the manuscript; MM and RC contributed to methodology, validation, and data curation; RC contributed to investigation and manuscript revision; LB conceived and supervised the study, provided resources, and contributed to methodology; MM and LB wrote the

manuscript and revised it; LB managed the project and acquired funding.

Peer review

The peer review history for this article is available at https://www.webofscience.com/api/gateway/wos/peer-review/10.1111/febs.70674.

Data availability Statement

All study data are included in the paper. Any additional data will be shared by the corresponding author upon request.

References

1 Lill R & Mühlenhoff U (2008) Maturation of iron-sulfur proteins in eukaryotes: mechanisms, connected processes, and diseases. *Annu Rev Biochem* **77**, 669–700. doi: 10.1146/annurev.biochem.76.052705.162653

2 Mühlenhoff U, Molik S, Godoy JR, Uzarska MA, Richter N, Seubert A, Zhang Y, Stubbe JA, Pierrel F, Herrero E *et al.* (2010) Cytosolic monothiol Glutaredoxins function in intracellular iron sensing and trafficking via their bound iron-sulfur cluster. *Cell Metab* **12**, 373–385. doi: 10.1016/j.cmet.2010.08.001

3 Rouault TA (2015) Mammalian iron–sulphur proteins: novel insights into biogenesis and function. *Nat Rev Mol Cell Biol* **16**, 45–55. doi: 10.1038/nrm3909

4 Rouault TA & Tong WH (2008) Iron–sulfur cluster biogenesis and human disease. *Trends Genet* **24**, 398–407. doi: 10.1016/j.tig.2008.05.008

5 Fuss JO, Tsai C-L, Ishida JP & Tainer JA (2015) Emerging critical roles of Fe–S clusters in DNA replication and repair. *Biochim Biophys Acta, Mol Cell Res* **1853**, 1253–1271. doi: 10.1016/j.bbamcr.2015.01.018

6 Read AD, Bentley RET, Archer SL & Dunham-Snary KJ (2021) Mitochondrial iron–sulfur clusters: structure, function, and an emerging role in vascular biology. *Redox Biol* **47**, 102164. doi: 10.1016/j.redox.2021.102164

7 Ciofi-Baffoni S, Nasta V & Banci L (2018) Protein networks in the maturation of human iron–sulfur proteins. *Metallomics* **10**, 49–72. doi: 10.1039/C7MT00269F

8 Braymer JJ, Stehling O, Stümpfig M, Rösser R, Spantgar F, Blinn CM, Mühlenhoff U, Pierik AJ & Lill R (2024) Requirements for the biogenesis of [2Fe-2S] proteins in the human and yeast cytosol. *Proc Natl Acad Sci USA* **121**, e2400740121. doi: 10.1073/pnas.2400740121

9 Wachnowsky C, Fidai I & Cowan JA (2018) Iron–sulfur cluster biosynthesis and trafficking – impact on human disease conditions. *Metallomics* **10**, 9–29. doi: 10.1039/C7MT00180K

10 Bandyopadhyay T & Outten CE (2022) The role of thiols in iron–sulfur cluster biogenesis. In Redox Chemistry and Biology of Thiolspp. 487–506. Elsevier, London. doi: 10.1016/B978-0-323-90219-9.00004-2

11 Schaedler TA, Thornton JD, Kruse I, Schwarzländer M, Meyer AJ, van Veen HW & Balk J (2014) A conserved mitochondrial ATP-binding cassette transporter exports glutathione polysulfide for cytosolic metal cofactor assembly. *J Biol Chem* **289**, 23264–23274. doi: 10.1074/jbc.M114.553438

12 Qi W, Li J & Cowan JA (2014) A structural model for glutathione-complexed iron–sulfur cluster as a substrate for ABCB7-type transporters. *Chem Commun* **50**, 3795–3798. doi: 10.1039/C3CC48239A

13 Li J & Cowan JA (2015) Glutathione-coordinated [2Fe–2S] cluster: a viable physiological substrate for mitochondrial ABCB7 transport. *Chem Commun* **51**, 2253–2255. doi: 10.1039/C4CC09175B

14 Pandey AK, Pain J, Dancis A & Pain D (2019) Mitochondria export iron-sulfur and sulfur intermediates to the cytoplasm for iron-sulfur cluster assembly and tRNA thiolation in yeast. *J Biol Chem* **294**, 9489–9502. doi: 10.1074/jbc.RA119.008600

15 Li H & Outten CE (2012) Monothiol CGFS Glutaredoxins and BolA-like proteins: [2Fe-2S] binding Partners in Iron Homeostasis. *Biochemistry* **51**, 4377–4389. doi: 10.1021/bi300393z

16 Li H, Mapolelo DT, Randeniya S, Johnson MK & Outten CE (2012) Human Glutaredoxin 3 forms [2Fe-2S]-bridged complexes with human BolA2. *Biochemistry* **51**, 1687–1696. doi: 10.1021/bi2019089

17 Haunhorst P, Berndt C, Eitner S, Godoy JR & Lillig CH (2010) Characterization of the human monothiol glutaredoxin 3 (PICOT) as iron–sulfur protein. *Biochem Biophys Res Commun* **394**, 372–376. doi: 10.1016/j.bbrc.2010.03.016

18 Lillig CH & Berndt C (2013) Glutaredoxins in thiol/disulfide exchange. *Antioxid Redox Signal* **18**, 1654–1665. doi: 10.1089/ars.2012.5007

19 Cuccaro R, Masini M, Malanho Silva J, Camponeschi F & Banci L (2026) Human glutaredoxin 3: multiple domains for a unique function. *J Inorg Biochem* **274**, 113103. doi: 10.1016/j.jinorgbio.2025.113103

20 Banci L, Camponeschi F, Ciofi-Baffoni S & Muzzioli R (2015) Elucidating the molecular function of human BOLA2 in GRX3-dependent Anamorsin maturation pathway. *J Am Chem Soc* **137**, 16133–16143. doi: 10.1021/jacs.5b10592

21 Mapolelo DT, Zhang B, Randeniya S, Albetel AN, Li H, Couturier J, Outten CE, Rouhier N & Johnson MK (2013) Monothiol glutaredoxins and A-type proteins: partners in Fe-S cluster trafficking. *Dalton Trans* **42**, 3107–3115. doi: 10.1039/C2DT32263C

22 Willems P, Wanschers BFJ, Esseling J, Szklarczyk R, Kudla U, Duarte I, Forkink M, Nooteboom M, Swarts H, Gloerich J *et al.* (2013) BOLA1 is an aerobic protein that prevents mitochondrial morphology changes induced by glutathione depletion. *Antioxid Redox Signal* **18**, 129–138. doi: 10.1089/ars.2011.4253
23 Banci L, Ciofi-Baffoni S, Gajda K, Muzzioli R, Peruzzini R & Winkelmann J (2015) N-terminal domains mediate [2Fe-2S] cluster transfer from glutaredoxin-3 to anamorsin. *Nat Chem Biol* **11**, 772–778. doi: 10.1038/nchembio.1892
24 Li H, Mapolelo DT, Dingra NN, Naik SG, Lees NS, Hoffman BM, Riggs-Gelasco PJ, Huynh BH, Johnson MK & Outten CE (2009) The yeast iron regulatory proteins Grx3/4 and Fra2 form heterodimeric complexes containing a [2Fe-2S] cluster with cysteinyl and Histidyl ligation. *Biochemistry* **48**, 9569–9581. doi: 10.1021/bi901182w
25 Ojeda L, Keller G, Mühlenhoff U, Rutherford JC, Lill R & Winge DR (2006) Role of Glutaredoxin-3 and Glutaredoxin-4 in the iron regulation of the Aft1 transcriptional activator in Saccharomyces cerevisiae. *J Biol Chem* **281**, 17661–17669. doi: 10.1074/jbc.M602165200
26 Kumánovics A, Chen OS, Li L, Bagley D, Adkins EM, Lin H, Dingra NN, Outten CE, Keller G, Winge D *et al.* (2008) Identification of FRA1 and FRA2 as genes involved in regulating the yeast iron regulon in response to decreased mitochondrial iron-sulfur cluster synthesis. *J Biol Chem* **283**, 10276–10286. doi: 10.1074/jbc.M801160200
27 Camponeschi F, Prusty NR, Heider SAE, Ciofi-Baffoni S & Banci L (2020) GLRX3 acts as a [2Fe–2S] cluster chaperone in the cytosolic iron–sulfur assembly machinery transferring [2Fe–2S] clusters to NUBP1. *J Am Chem Soc* **142**, 10794–10805. doi: 10.1021/jacs.0c02266
28 Bargagna B, Matteucci S, Ciofi-Baffoni S, Camponeschi F & Banci L (2023) Unraveling the mechanism of [4Fe-4S] cluster assembly on the N-terminal cluster binding site of NUBP1. *Protein Sci* **32**, e4625. doi: 10.1002/pro.4625
29 Netz DJA, Stith CM, Stümpfig M, Köpf G, Vogel D, Genau HM, Stodola JL, Lill R, Burgers PMJ & Pierik AJ (2012) Eukaryotic DNA polymerases require an iron-sulfur cluster for the formation of active complexes. *Nat Chem Biol* **8**, 125–132. doi: 10.1038/nchembio.721
30 Stehling O, Netz DJA, Niggemeyer B, Rösser R, Eisenstein RS, Puccio H, Pierik AJ & Lill R (2008) Human Nbp35 is essential for both cytosolic iron-sulfur protein assembly and iron homeostasis. *Mol Cell Biol* **28**, 5517–5528. doi: 10.1128/MCB.00545-08
31 Rey P, Taupin-Broggini M, Couturier J, Vignols F & Rouhier N (2019) Is there a role for Glutaredoxins and BOLAs in the perception of the cellular iron status in plants? *Front Plant Sci* **10**, 712. doi: 10.3389/fpls.2019.00712
32 Sen S & Cowan JA (2017) Role of protein-glutathione contacts in defining glutaredoxin-3 [2Fe–2S] cluster chirality, ligand exchange and transfer chemistry. *JBIC J Biol Inorg Chem* **22**, 1075–1087. doi: 10.1007/s00775-017-1485-9
33 Trnka D, Hossain MF, Jordt LM, Gellert M & Lillig CH (2020) Role of GSH and iron-sulfur Glutaredoxins in iron metabolism—review. *Molecules* **25**, 3860. doi: 10.3390/molecules25173860
34 Berndt C, Lillig CH & Holmgren A (2007) Thiol-based mechanisms of the thioredoxin and glutaredoxin systems: implications for diseases in the cardiovascular system. *Am J Physiol Heart Circ Physiol* **292**, H1227–H1236. doi: 10.1152/ajpheart.01162.2006
35 Sviderskiy VO, Terzi EM & Possemato R (2019) Iron–sulfur cluster metabolism impacts iron homeostasis, ferroptosis sensitivity, and human disease. In Ferroptosis in Health and Diseasepp. 215–237. Springer International Publishing, Cham. doi: 10.1007/978-3-030-26780-3_12
36 Camponeschi F, Ciofi-Baffoni S, Calderone V & Banci L (2022) Molecular basis of rare diseases associated to the maturation of mitochondrial [4Fe-4S]-containing proteins. *Biomolecules* **12**, 1009. doi: 10.3390/biom12071009
37 Netz DJA, Pierik AJ, Stümpfig M, Bill E, Sharma AK, Pallesen LJ, Walden WE & Lill R (2012) A bridging [4Fe-4S] cluster and nucleotide binding are essential for function of the Cfd1-Nbp35 complex as a scaffold in iron-sulfur protein maturation. *J Biol Chem* **287**, 12365–12378. doi: 10.1074/jbc.M111.328914
38 Pallesen LJ, Solodovnikova N, Sharma AK & Walden WE (2013) Interaction with Cfd1 increases the kinetic lability of FeS on the Nbp35 scaffold. *J Biol Chem* **288**, 23358–23367. doi: 10.1074/jbc.M113.486878
39 Netz DJA, Pierik AJ, Stümpfig M, Mühlenhoff U & Lill R (2007) The Cfd1–Nbp35 complex acts as a scaffold for iron-sulfur protein assembly in the yeast cytosol. *Nat Chem Biol* **3**, 278–286. doi: 10.1038/nchembio872
40 Stehling O, Jeoung J-H, Freibert SA, Paul VD, Bänfer S, Niggemeyer B, Rösser R, Dobbek R & Lill R (2018) Function and crystal structure of the dimeric P-loop ATPase CFD1 coordinating an exposed [4Fe-4S] cluster for transfer to apoproteins. *Proc Natl Acad Sci USA* **115**, E9085–E9094. doi: 10.1073/pnas.1807762115
41 Wachnowsky C, Fidai I & Cowan JA (2016) Cytosolic iron–sulfur cluster transfer—a proposed kinetic pathway for reconstitution of glutaredoxin 3. *FEBS Lett* **590**, 4531–4540. doi: 10.1002/1873-3468.12491

42 Philpott CC & Ryu M-S (2014) Special delivery: distributing iron in the cytosol of mammalian cells. *Front Pharmacol* **5**, 173. doi: 10.3389/fphar.2014.00173

43 Frey AG, Palenchar DJ, Wildemann JD & Philpott CC (2016) A glutaredoxin·BolA complex serves as an iron-sulfur cluster chaperone for the cytosolic cluster assembly machinery. *J Biol Chem* **291**, 22344–22356. doi: 10.1074/jbc.M116.744946

44 Fan X, Barshop WD, Vashisht AA, Pandey V, Leal S, Rayatpisheh S, Jami-Alahmadi Y, Sha J & Wohlschlegel JA (2022) Iron-regulated assembly of the cytosolic iron-sulfur cluster biogenesis machinery. *J Biol Chem* **298**, 102094. doi: 10.1016/j.jbc.2022.102094